Mineralogical Magazine, December 2006, Vol. 70(6), pp. 709–729

A survey of accessory mineral assemblages in peralkaline and more aluminous A-type granites of the southeast coastal area of China

L. XIE, R. C. WANG*, D. Z. WANG AND J. S. QIU

State Key Laboratory for Mineral Deposits Research, Department of Earth Sciences, Nanjing University, Nanjing 210093, P. R. China

ABSTRACT

An extensive belt of A-type granite exists along the southeast coast of China. The granites are divided into peralkaline and more aluminous subgroups which differ in mineral assemblages, mineral compositions and textures. In the peralkaline subgroup, primary magmatic Th-rich zircon is typically overgrown by Th-poor zircon containing thorite micro-inclusions. *REE* minerals in this subgroup are dominated by allanite-(Ce), chevkinite-(Ce), titanite and pyrochlore. Fe-Ti oxides are titanian magnetite and Mn-rich ilmenite. In contrast, in the more aluminous subgroup rocks, zircon is weakly zoned and exhibits very low Th but relatively high U contents. The *REE* minerals are dominated by Th-rich monazite-(Ce). Titanium-poor magnetite, pyrophanite and rutile are the major Fe-Ti oxides. These occurrences indicate that peralkaline magmas favour the formation of *REE* silicates, whereas magmas with higher alumina saturation stabilize *REE* phosphates. Peralkaline granites crystallized at temperatures 50–100ºC greater than the more aluminous granites, but under lower oxidation conditions. These differences in formation conditions of the two A-type granite subgroups, deduced by accessory mineral characteristics, are inferred to be related to magma derivation at different crustal levels, with peralkaline magma deriving from a deeper crustal level with more mantle input.

KEYWORDS: A-type granite, peralkaline, aluminous, accessory minerals, *REE*, China.

Introduction

AN extensive belt of A-type granite exists along the southeast coast of China (Wang *et al.*, 1995) and is divided into peralkaline (PA) and aluminous (AA) subgroups on the basis of mineralogical, textural and geochemical features (Qiu *et al.*, 2004). In spite of previous investigation, issues remain regarding their petrogenesis: (1) are coexisting PA and AA subgroups representative of distinct geological settings, sources, or physicochemical conditions of formation, and (2) if distinct, what accounts for the observed mineralogical, textural, and compositional diversity? In this paper, we compare the accessory mineral suites of the two A-type subgroups and make inferences on the physicochemical conditions, magmatic evolution, and tectonic settings of the two subgroups. Previous studies focused on the geochemistry of these granites and few data exist on the accessory minerals in these regionally significant rocks. Given that the occurrence and stability of accessory minerals is dependent upon a range of important parameters, most notably temperature, magma composition and f_{O_2}, this paper is a contribution to our understanding of these rocks from southeastern China and of accessory mineral occurrences in general.

* E-mail: rcwang@nju.edu.cn
DOI: 10.1180/0026461067060362

Geological setting and sample description

Post-orogenic A-type granites are widely distributed in the southeastern coastal region of China, from Fujian Province in the south to Shandong Province in the north (Fig. 1; Tu *et al.*, 1982). The granites are related to the Cretaceous orogeny from 130−90 Ma (Zhou and Li, 2000). Eight

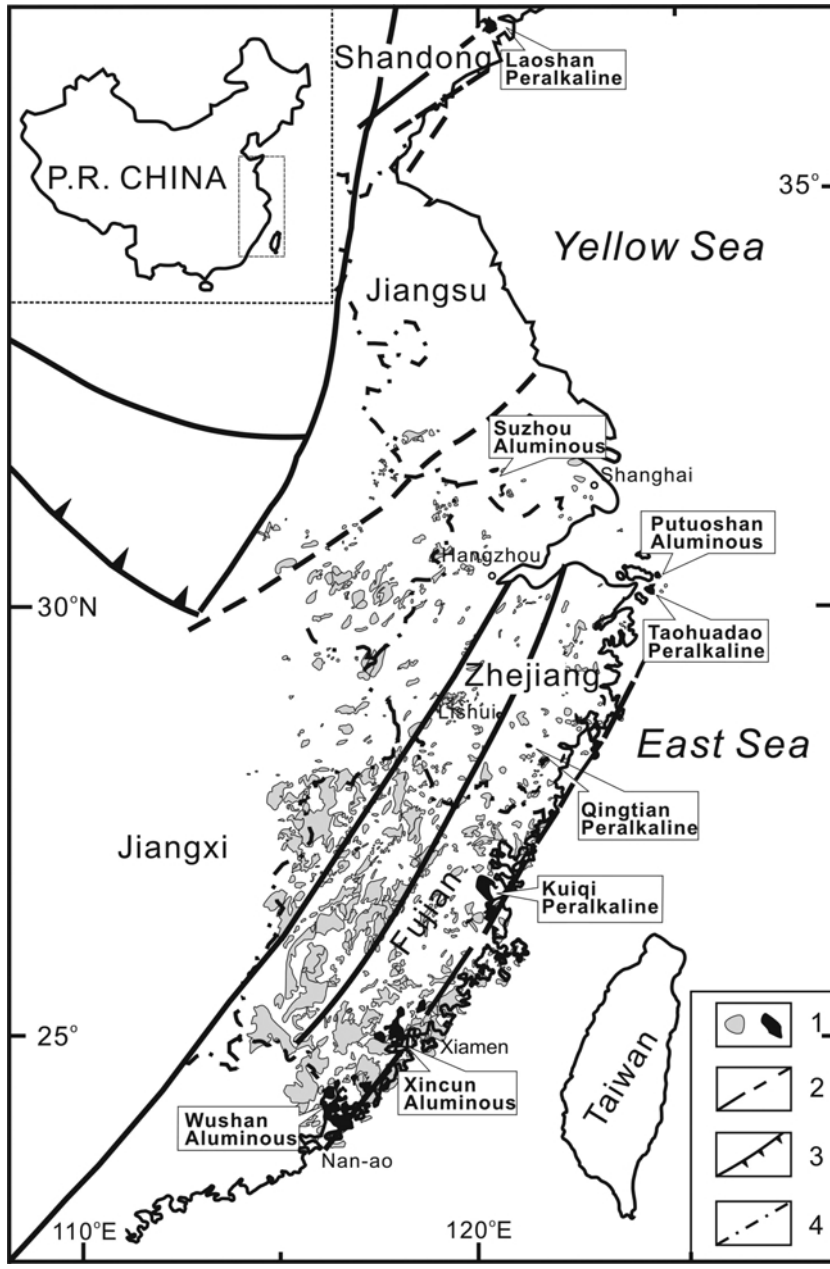

FIG. 1. Simplified geological map showing the outcrop distribution of A-type granites of the southeast coastal area of China. Province names are shown. Key: 1 − A-type granite (black fill, studied PA and AA subgroup; grey shading, granites); 2 − fault zone; 3 − tectonic suture zone; 4 − provincial boundary.

previously studied granites were selected for this study: the Laoshan, Taohuadao, Qingtian and Kuiqi peralkaline (PA) granites and the Suzhou, Putuoshan, Xincun and Wushan aluminous (AA) granites; sample locations are shown in Fig. 1.

Peralkaline A-type (PA) granite subgroup

The Laoshan PA granite occurs in the eastern extension region of the Dabie ultra-high pressure (UHP) orogenic belt (Wang *et al.*, 2000). It is mainly an arfvedsonite-bearing alkali feldspar granite occupying the eastern part of the Qingdao I- and A-type composite granitic batholith which has an outcrop area of 600 km^2. Arfvedsonite-filled miarolitic cavities are common. The Taohuadao alkali feldspar granite pluton crops out in southern Taohua Island, Zhejiang Province. Structurally, it occurs at the northeast margin of the NNE-trending Zhenhai–Wenzhou thrust fault. According to Qiu *et al.* (1996), this post-orogenic A-type granite marks the end of Cretaceous orogeny in southeastern China. Miarolitic cavities are fairly common. The Qingtian PA granite is a lens-shaped body elongated in a northeasterly direction. Like the two granites already mentioned, it belongs to the miarolitic alkali feldspar granitic belt of the east coast area of China (Peng and Dong, 1991). The Kuiqi PA granite is spatially associated with I-type calc-alkaline granites (Tu *et al.*, 1982; Martin *et al.*, 1994). It is a leucocratic alkali feldspar-rich rock with a coarse- to medium-grained texture. Common miarolitic cavities are filled with quartz, alkali feldspar and arfvedsonite. Generally, the typical rock-forming mineral assemblage for the PA granites is quartz, mesoperthite, sodic amphibole (magnesio-arfvedsonite to arfvedsonite) and sodic pyroxene (aegirine) (Table 1).

Aluminous A-type (AA) granite subgroup

The aluminous A-type Suzhou granite is a medium-grained biotite-bearing granite (Wang *et al.*, 1996; Wei *et al.*, 2000). Common miarolitic cavities, mm to tens of cm across, are well developed and filled by clusters of quartz and alkali feldspar. The Putuoshan AA granite crops out at Putuo Island, Zhejiang Province. Enclaves of quartz diorite range from 0.5 to 5 m in diameter. Abundant miarolitic cavities are filled with quartz, K-feldspar and spessartine. With an outcrop area of 79.2 km^2, the Xincun AA granite is located in East Zhangzhou City, Fujian Province. It is mainly medium to coarse-grained, with a fine-grained marginal facies. Miarolitic cavities are filled with quartz clusters, pink-coloured alkali feldspar, white-coloured muscovite and abundant reddish-brown spessartine (Zhou and Wu, 1994). Similar to the Xincun AA granite, the Wushan AA granite is also medium- to coarse-grained and contains abundant miarolitic cavities filled with the same assemblage as the Xincun AA granite. Generally, the typical rock-forming mineral assemblage for the AA granites is quartz, mesoperthite, Fe-Ca or Na-Ca amphibole, and biotite (Table 1).

Whole-rock geochemistry

Data in this section of the text are from Qiu *et al.* (2004). Geochemically, the two subgroups of granite are both silica-saturated (~77 wt.% SiO_2), with high total alkalis ($K_2O + Na_2O \geqslant 8.5$ wt.%), and low Fe_2O_3 (0.40–1.54 wt.%), FeO (0.04–1.19 wt.%), MgO (0.01–0.40 wt.%), and CaO (<0.01–0.96 wt.%). In comparison with PA granites, AA granites are more aluminous with Al_2O_3 contents generally >12 wt.% and ANK [mol. $Al_2O_3/(Na_2O+K_2O)$] generally >1. In a plot

TABLE 1. Summary of rock-forming mineral assemblages in the two A-type granite subgroups, southeast coastal area of China.

	Peralkaline subgroup (PA)	Aluminous subgroup (AA)
Feldspar	Alkali feldspar	Alkali feldspar, K-feldspar
Amphibole	Arfvedsonite, magnesio-arfvedsonite	Fe-Ca amphibole, Na-Ca amphibole
Pyroxene	Aegirine	Ca-Fe pyroxene
Mica	Absent	Biotite, annite
In miarolitic cavities	Quartz, K-feldspar, arfvedsonite, aegirine, zircon, fluorite	Quartz, K-feldspar, muscovite, spessartine, fluorite

of ANK *vs.* ACNK [mol. Al_2O_3/($CaO+Na_2O+K_2O$)], the AA granites mainly plot in the metaluminous and weakly peraluminous fields, whereas the PA granites mostly fall into the peralkaline field with a few that are metaluminous (Fig. 2*a*).

PA and AA granites have similar rare earth element (*REE*) and trace-element patterns. They are moderately fractionated in the light *REE*, but have approximately flat to slightly enriched heavy *REE* chondrite normalized patterns. Both types of granite have a pronounced negative Eu anomaly. The total *REE* content is slightly enriched in some PA granites. Relative to AA granites, the PA granites are significantly depleted in Sr, Ba, P and Ti, but enriched in Rb, Th and U. The high Ga/Al ratio of PA granites is diagnostic for this subgroup. In summary, the PA and AA granites have only slight differences in trace-element characteristics (Qiu *et al.*, 2004), yet it is possible to geochemically distinguish the two subgroups (Fig. 2*b,c*).

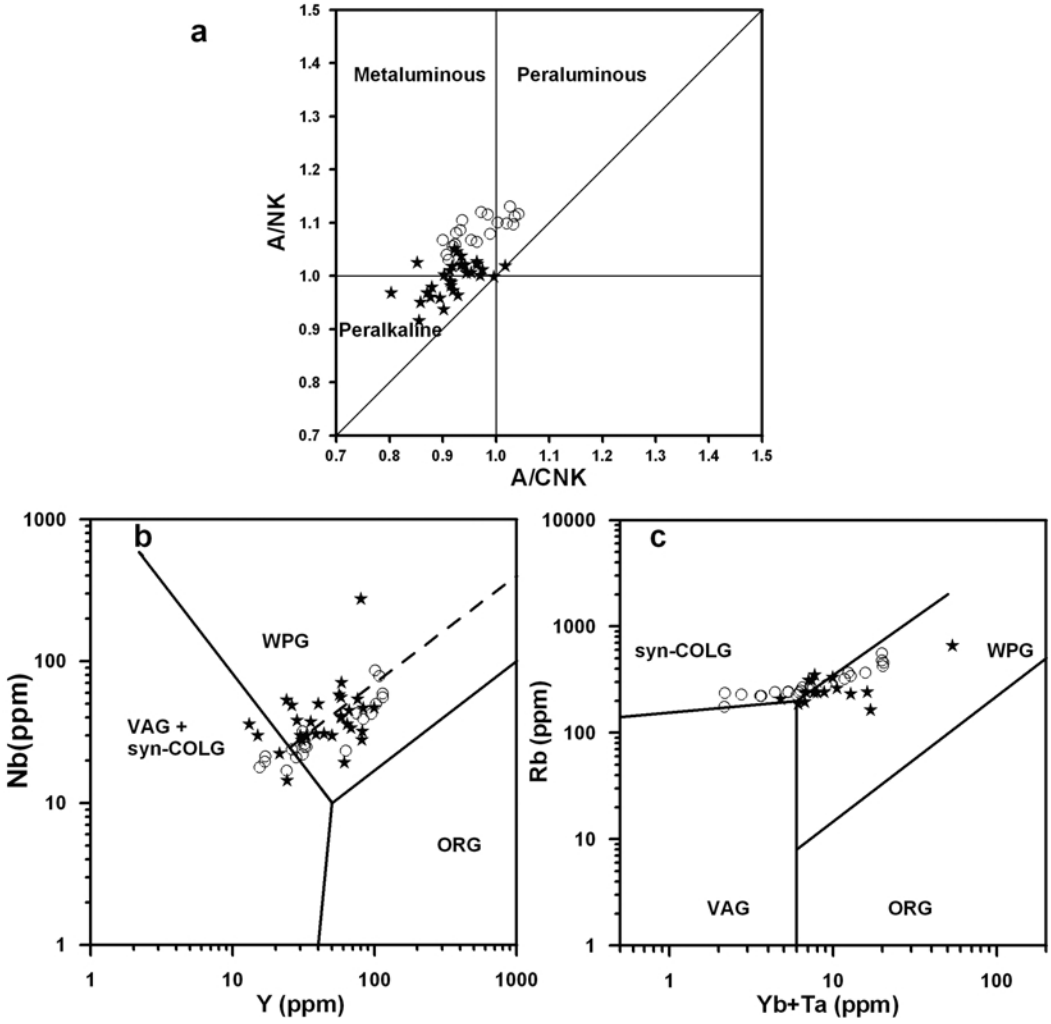

FIG. 2. Whole-rock compositional plots for A-type granites from southeastern coastal China (data from Qiu *et al.*, 2004). Symbols: open circles, AA subgroup; solid star, PA subgroup. (*a*) ANK *vs.* ACNK plot. (*b*) Nb *vs* Y discrimination diagram. (*c*) Rb *vs.* Yb+Ta discrimination diagram. A/NK = $Al_2O_3/(Na_2O + K_2O)$, A/CNK = $Al_2O_3/(Na_2O + K_2O + CaO)$. Syn-COLG = syn-collision granites, VAG = volcanic-arc granites, WPG = within-plate granites, ORG = ocean-ridge granites. Plots of *b* and *c* after Pearce (1984).

Analytical methods

Back-scattered electron (BSE) images, quantitative analysis, and element mapping were carried out on polished thin sections using a JEOL JXA-8800M electron microprobe at the State Key Laboratory for Mineral Deposits Research, Nanjing University. Operating conditions were: accelerating voltage 20 kV, probe current 20 nA for Zr-Th-U silicates and *REE* minerals, and 15 kV and 20 nA for Fe-Ti oxide minerals. In order to obtain the best quality BSE images, the accelerating voltage at times was set at 15 kV when capturing the images. For quantitative wavelength dispersive spectrometry-electron microprobe analysis (EMPA), the counting time on peaks was 10 s for major elements and 20–60 s for minor elements (*REE* and trace elements). Counting times on the background were half those intervals. The diameter of the electron beam was ~1 μm. All data were corrected with standard ZAF correction procedures. Synthetic Y and *REE* pentaphosphates [YP_5O_{14} and (REE)P_5O_{14}] were used as standards. Details of standards and analytical methods used to reduce the spectral overlaps involving U, Th and other elements are the same as those described by Wang *et al.* (2003) and Zhang *et al.* (2004).

Due to the relatively complicated spectral overlap corrections required for accurate analysis of *REE*-rich minerals, replicate analyses of selected allanite and monazite grains were performed by electron microprobe analysis by Dr de Parseval at the Laboratoire de Mecanismes de transfert en Geologie, Université Paul Sabatier, France. Analytical conditions were: accelerating voltage 15 kV, probe current 20 nA, counting time on peaks 10 s except for uranium (50 s). Counting times on the background were half those intervals and 50 s for uranium. Replicate analyses confirmed the integrity of data collected by the Nanjing JEOL probe.

Accessory minerals: texture and composition

Zircon

Although zircon in the PA and AA granites occur in interstices between earlier-formed minerals (Fig. 3), differences in morphology, internal structure, and composition are observable and are described according to granite subgroup (PA and AA) below.

Zircon in PA granites

The phase occurs as subhedral to anhedral crystals. It is 100–200 μm long, rarely up to 1.2 mm. In BSE images, zircon is markedly heterogeneous in composition and in the distribution of thorite inclusions. Generally, the margin of individual crystals is less Th-rich than the core, but contains significantly more inclusions of thorite and is porous (Fig. 3*a*–*d*). Amoeboid veinlets of zircon can be observed in the marginal parts of some zircon grains (Fig. 3*a*,*b*) and they penetrate into adjacent ilmenite like 'stringers' (Fig. 3*b*). The EMPA-determined compositions of zircon are given in Table 2. The HfO_2 content ranges from 0.93 to 2.96 wt.%. In BSE images, the brighter central portions are more enriched in Th ($2 < ThO_2 < 11$ wt.%; $1 < ThO_2/UO_2 < 100$), whereas the ThO_2 content in the marginal part is generally <1 wt.%, with ThO_2/UO_2 values varying from 0 to 15 (Fig. 4).

Zircon in AA granites

Zircon in AA granites occurs mainly as subhedral to euhedral grains ~100 μm across. The crystals have simple zoning (Fig. 3*e*) and occur with thorite and columbite (Fig. 3*f*). Electron microprobe data (Table 2) show that HfO_2 values mostly range between 2.03 and 5.92 wt.%, but can be as high as 11.05 wt.%. The abundance of Y_2O_3 is highly variable, from below detection (Suzhou and Wushan granites) to 3.59 wt.% (Putuoshan and Xincun granites). Thorium oxide is mostly <1 wt.%, except in zircon from the Putuoshan AA granite (1.07–2.55 wt.%). The concentration of UO_2 is up to 4.34 wt.% and the ThO_2/UO_2 ratio is generally <0.5 (Fig. 4).

REE minerals

Allanite-(Ce)

This phase is only present in the PA granites. It is commonly found in the Qingtian granite and to a lesser extent in the Kuiqi and Taohuadao granites. It is absent from the Laoshan granite. Allanite typically occurs as subhedral to euhedral crystals and exhibits oscillatory zoning (Fig. 5*a*), or occurs as aggregates together with Fe-Ti oxides in interstices of the rock-forming silicates. As shown by EPMA data (Table 3), the preserved zones of allanite-(Ce) show increasing Ce_2O_3, La_2O_3 and FeO contents from core to rim, whereas CaO and Al_2O_3 decrease along the section. The highest contents of Ce_2O_3, La_2O_3 and FeO are 11.83, 7.24 and 23.27 wt.%,

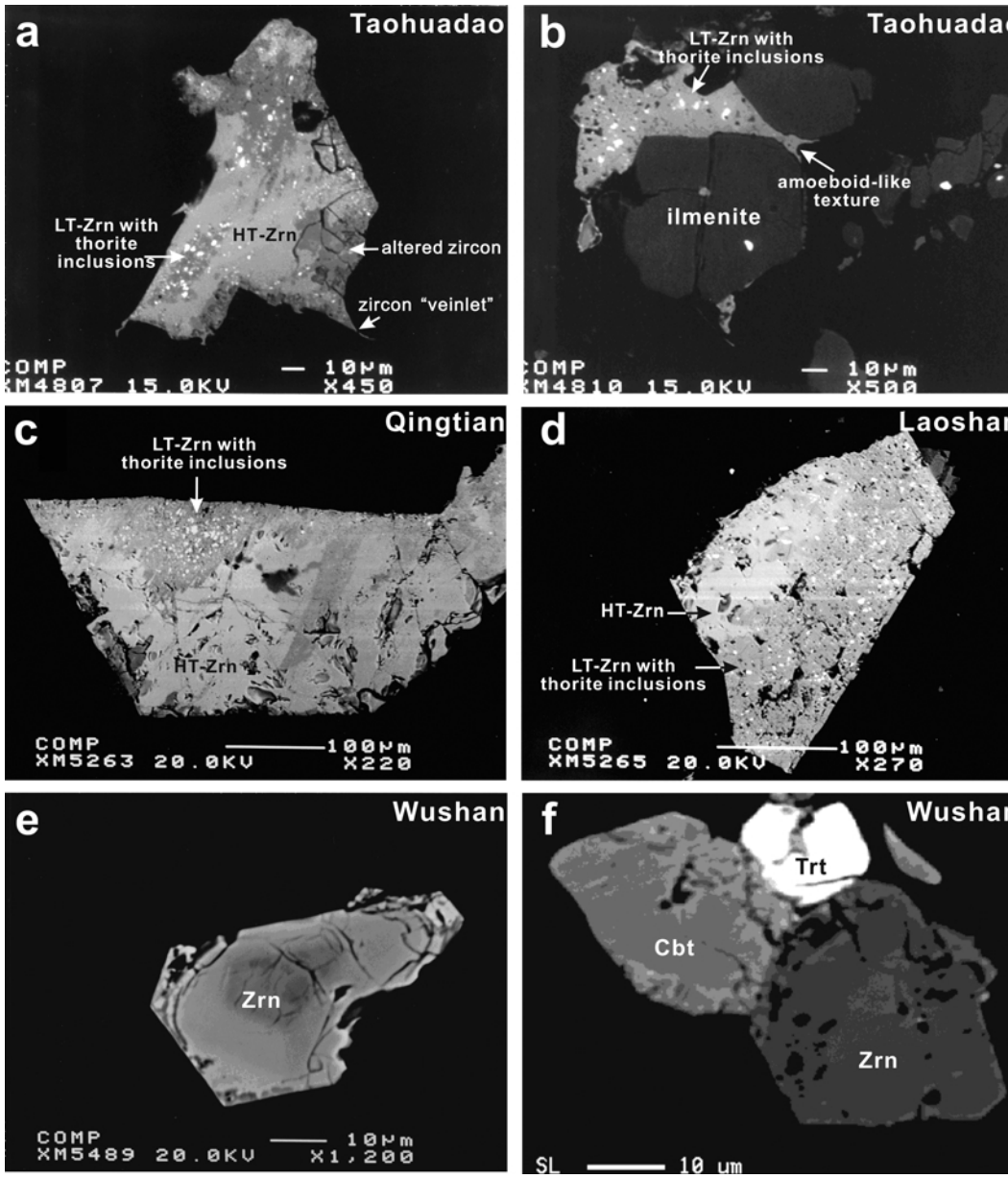

FIG. 3. Series of backscattered electron images of zircon from A-type granites from southeastern coastal China. Granite name is given in the top-right corner of each image. PA subgroup samples: Taohuadao, Qingtian, Laoshan; AA subgroup sample: Wushan. Mineral abbreviations: LT-Zrn = low-Th zircon; HT-Zrn = high-Th zircon; Trt = thorite; Cbt = columbite.

respectively. Allanite zoning is probably a combination of the coupled substitution $REE^{3+} + Fe^{2+} \rightarrow Ca^{2+} + Fe^{3+}$ and whole-rock *REE* fractionation as Casillas *et al.* (1995) have shown.

Chevkinite-(Ce)

Like allanite-(Ce), chevkinite-(Ce) is only found in the PA granites (Qingtian, Kuiqi and Taohuadao). It typically occurs as stubby euhedral,

TABLE 2. Electron microprobe analyses (wt.%) of zircon from A-type granites, southeast coastal area of China.

	Peralkaline (PA) A-type granites										
	— Taohuadao —			— Qingtian —			– Laoshan –		—— Kuiqi ——		
Th-rich zircon											
	1	2	3	4	5	6	7	8	9	10	11
P_2O_5	0.18	0.13	0.06	0.11	0.24	–	1.40	1.71	0.02	0.03	0.14
SiO_2	29.58	29.31	30.46	31.73	31.87	33.17	30.04	30.10	31.12	31.46	32.15
ZrO_2	57.47	55.87	57.93	54.84	51.80	54.23	60.07	58.95	61.14	56.90	57.39
HfO_2	2.32	2.39	2.39	0.93	0.97	2.96	1.41	1.60	2.06	2.04	1.65
ThO_2	7.24	10.10	6.89	6.53	7.17	6.36	3.55	3.37	2.25	2.68	2.21
UO_2	0.02	0.72	0.53	2.86	3.04	1.71	0.39	0.37	1.50	1.44	1.79
Y_2O_3	0.48	0.42	0.52	2.89	3.14	0.14	2.94	2.62	1.16	1.25	1.94
PbO	–	0.08	0.05	–	–	0.02	n.a.	n.a.	0.11	0.12	0.16
Total	97.29	99.02	98.83	99.90	98.22	98.58	99.8	98.72	99.38	95.93	97.43
Th-poor zircon											
	12	13	14	15	16	17	18	19	20	21	22
P_2O_5	0.09	0.02	–	0.02	–	–	–	0.56	0.01	0.08	0.01
SiO_2	32.37	33.04	30.72	31.75	32.51	32.51	32.78	31.31	32.99	32.56	32.79
ZrO_2	65.65	61.87	66.04	60.53	64.75	64.75	65.26	63.50	63.13	61.12	62.54
HfO_2	1.31	3.31	2.88	7.31	2.22	2.22	1.98	1.95	1.92	3.31	1.93
ThO_2	–	0.87	0.11	0.08	0.00	0.00	0.05	0.31	0.02	0.01	0.06
UO_2	0.23	0.08	0.04	0.31	0.04	0.04	0.01	0.15	0.09	0.45	0.15
Y_2O_3	–	0.13	0.02	0.00	0.00	0.00	0.03	1.11	0.21	0.42	0.14
PbO	–	0.01	–	–	–	–	0.05	n.a. .	–	0.07	–
Total	99.64	99.32	99.81	99.99	99.52	99.52	100.15	98.89	98.36	98.00	97.61

	Aluminous (AA) A-type granites										
	— Putuoshan —			— Suzhou —			— Xincun —			– Wushan –	
	23	24	25	26	27	28	29	30	31	32	33
P_2O_5	0.30	0.59	0.27	0.02	0.06	0.21	0.52	0.40	0.26	0.06	–
SiO_2	30.40	29.65	30.23	30.05	30.89	31.37	32.69	30.14	31.35	30.49	31.40
ZrO_2	53.42	52.84	56.62	60.6	60.86	60.70	58.97	62.00	56.57	61.32	57.51
HfO_2	3.16	3.78	3.95	4.94	5.92	5.32	2.08	2.03	3.86	2.99	11.05
ThO_2	2.55	1.93	1.07	0.38	0.16	0.08	0.79	0.84	0.60	0.44	0.01
UO_2	4.34	4.19	2.70	1.20	0.31	0.20	1.02	1.32	2.39	2.46	0.01
Y_2O_3	2.70	3.59	1.79	0.30	0.39	0.16	2.01	1.83	1.95	0.77	–
PbO	0.10	0.19	0.02	n.a.	n.a.	n.a.	–	0.04	0.03	0.06	–
Total	96.97	96.75	96.63	97.49	98.59	98.04	98.08	98.61	97.01	98.59	99.97

–: below detection limit (Th: 100 ppm; U: 100 ppm; Y: 200 ppm; P: 100 ppm; Pb: 200 ppm)
n.a.: not analysed.

zoned crystals. Chevkinite-(Ce) is most often intergrown with zircon (Fig. 5*b*), fluorite, apatite and ilmenite. In the Qingtian PA granite, chevkinite-(Ce) is rimmed and partially replaced by bastnäsite-(Ce). Overall, the analysed chevkinite-(Ce) contains up to 24.11 wt.% Ce_2O_3, 18.46 wt.% TiO_2, 17.44 wt.% La_2O_3, and 10.57 wt.% FeO. They are in the same level as those in the Shuiquangou syenite of northern China (21.5 wt.% Ce_2O_3, 10.3 wt.% La_2O_3, 9.7 wt.% FeO) (Jiang, 2006) and that in peralkaline rhyolitic magmas from Gran Canaria in Spain (22.3 wt.% Ce_2O_3, 13.8 wt.% La_2O_3, 9.4 wt.% FeO) (Troll *et al.*, 2003). It also contains 1.02–2.39 wt.% Pr_2O_3 and 1.54–9.17 wt.% Nd_2O_3 (Table 3), similar to the levels in chevkinite-(Ce) from the Shuiquangou syenite and rhyolitic magmas (both are 2.0 wt.% Pr_2O_3 and 7.5 wt.% Nd_2O_3). Some grains have low

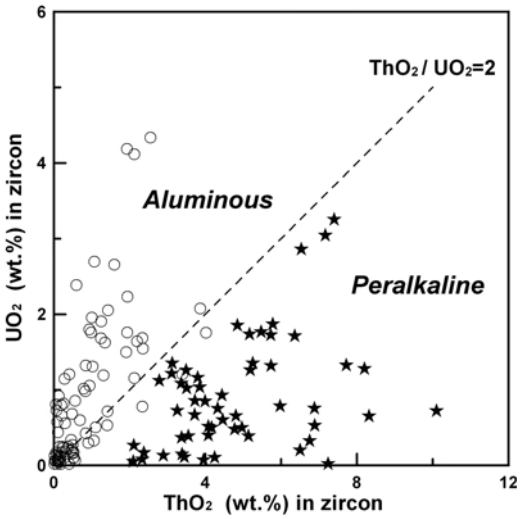

FIG. 4. ThO_2 *vs.* UO_2 plot for zircon from peralkaline (PA) and aluminous (AA) A-type granite subgroups from southeastern coastal China. Symbols: open circles – AA subgroup; solid star – PA subgroup.

oxide totals, probably exhibiting extensive metamictization.

Titanite

Wang *et al.* (2001) describe euhedral to subhedral titanite in the Laoshan PA granite (Fig. 5*c*). In the present study, titanite occurs as sporadic inclusions in quartz and K-feldspar in the Kuiqi and Taohuadao PA granites. It contains up to 1.7 and 0.4 wt.% Ce_2O_3 and La_2O_3, respectively. Titanite in the Laoshan PA granite is enriched in Nb_2O_5 (up to 2.2 wt.%) and Y_2O_3 (up to 1.8 wt.%) (Table 4). Titanite is also found in the Putuoshan and Xincun AA granites, associated with alteration minerals such as fluorite and fluocerite. Compositionally, it is enriched in Al with the highest Al_2O_3 of 9.4 wt.% in titanite from the Putuoshan granite. The *REE* concentrations are low with the total REE_2O_3 generally <1 wt.%.

Pyrochlore

This phase only occurs in interstices in the Kuiqi and Laoshan PA granites. Grains vary from ~100 to 400 μm across. Pyrochlore is zoned, with three distinctive compositions (Pyc-I, Pyc-II and Pyc-III) (Fig. 5*d*). Pyc-I in the core is mantled by Pyc-II which is typically fissured, with Pyc-III forming the outermost zone. The EMPA results, shown in Table 5, indicate that the three zones plot within the pyrochlore subgroup field in Fig. 6*a*, but they have distinctive contents of Na, Ca, U and Pb at the A site (Fig. 6*b*). In addition to Na and Ca, Pyc-I also contains 12–14 wt.% UO_2. With respect to Pyc-I, the Na, Ca and U contents in Pyc-II decrease and Pb is enriched, to a level justifying the term plumbopyrochlore. The largest values of Pb occur in Pyc-III, with PbO up to 57.3 wt.%, whereas the Na, Ca, U and Th contents are low. Thus the Pyc-III part can also be considered as a typical plumbopyrochlore. The fissured texture of Pyc-II suggests significant metamictization, consistent with low oxide totals (Table 5).

Monazite-(Ce)

Monazite occurs as anhedral grains up to 200 μm across in AA granites, commonly enclosed in quartz and feldspar (Fig. 5*e*), or forming aggregates together with zircon, ilmenite and xenotime. Occasionally, monazite crystals are replaced by fluocerite (Fig. 5*f*). Monazite-(Ce) is enriched in Th, with 8.2–25.5 wt.% ThO_2 (Table 6). The rim may contain up to 26.5 wt.% ThO_2 in the Wushan granite (Fig. 5*e*). The monazite contents measured in this study are similar to the monazite contents in the peraluminous S-type granite (ThO_2 in the range 6–12 wt.%, Cuney and Friedrich, 1987; 4–12 wt.%, Förster, 1998*a*; 4.1–10.7 wt.%, Wang *et al.*, 2003). Monazite-(Ce) is rare in PA granites and is associated with zircon, fluorite, bastnäsite-(Ce) or fluocerite. Unlike AA granites, monazite-(Ce) in PA granites contains particularly low Th (0.3–1.0 wt.%) (Table 6). La_2O_3 and Ce_2O_3 are more abundant at 13–24 wt.% and ~38 wt.%, respectively. Other *LREE*s vary within limited ranges, e.g. Pr_2O_3 (2.5–4.0 wt.%), Nd_2O_3 (3.3–8.7 wt.%) and Sm_2O_3 (0.1–1.7 wt.%).

Bastnäsite-(Ce)

This phase occurs as anhedral grains (40–80 μm) in both granite subgroups and forms aggregates with other *REE* minerals and Fe-Ti oxides in interstices. It replaces allanite-(Ce) and monazite-(Ce) (Fig. 5*b*,*f*).

Fe-Ti oxide minerals

Magnetite

This phase occurs as anhedral grains in interstices in the two A-type granite subgroups, and usually forms aggregates with ilmenite (Table 7, Fig. 7*a*). The magnetite can be compositionally divided into the two subgroups. Magnetite

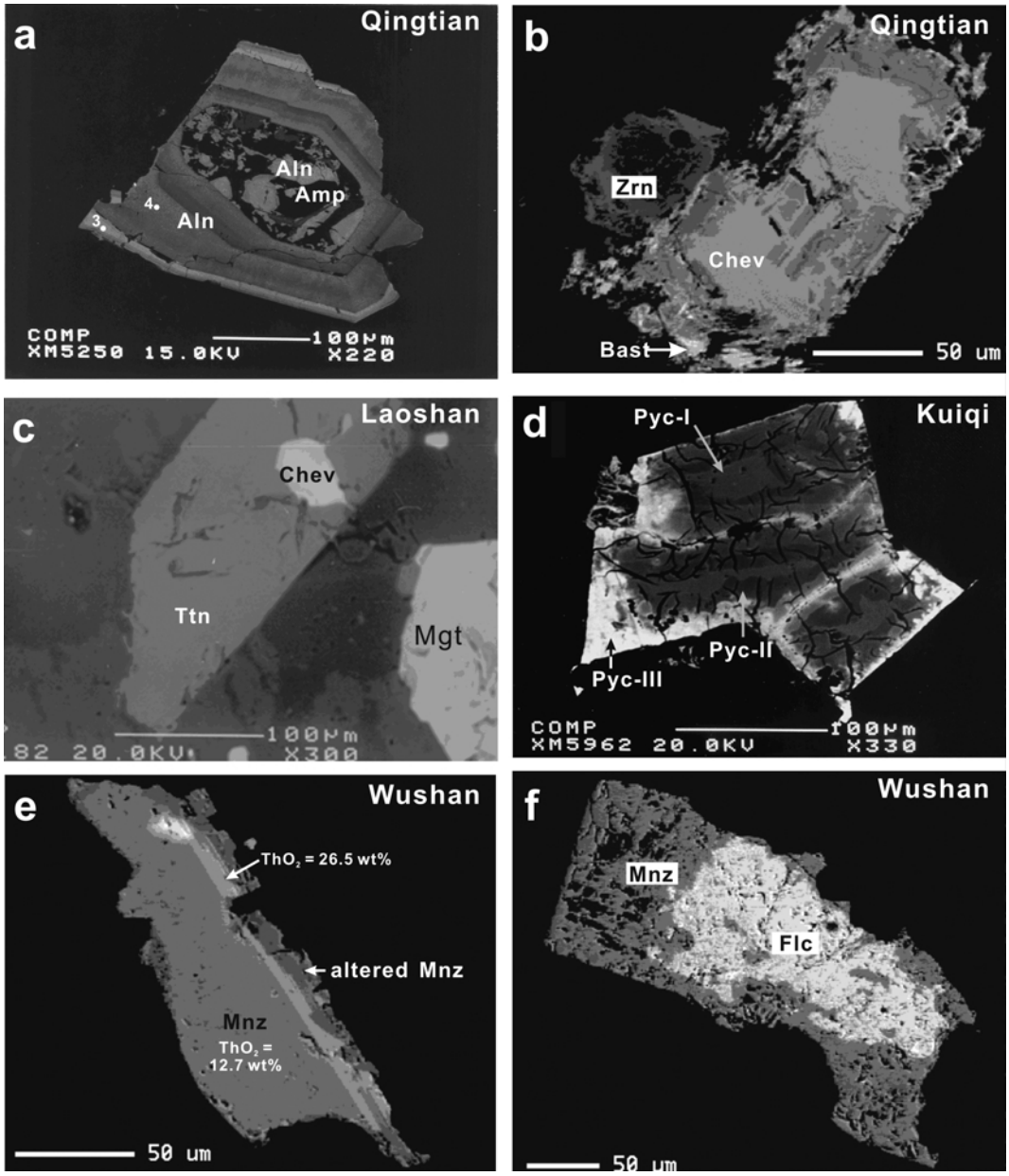

FIG. 5. Series of backscattered electron images of *REE* minerals from A-type granites from southeastern coastal China. Granite name is given in the top-right corner of each image. PA subgroup samples: Qingtian, Laoshan, Kuiqi; AA subgroup sample: Wushan. (*a*) Intergrowth of amphibole and allanite mantled with well developed zoned allanite; the numbers on the crystal correspond to the analyses in Table 3. (*b*) Corroded chevkinite with the margin altered to bastnäsite-(Ce). (*c*) Inclusion of chevkinite in titanite. (*d*) Three types of pyrochlore, Pyc-II is fractured. (*e*) Monazite enriched in ThO_2 (up to 26.5 wt.%). (*f*) Fluocerite occurs as the alteration product of monazite. Mineral abbreviations: Aln = allanite; Amp = amphibole; Bast = bastnäsite; Chev = chevkinite; Zrn = zircon; Pyc = pyrochlore; Ttn = titanite; Mgt = magnetite; Mnz = monazite; Flc = fluocerite.

TABLE 3. Electron microprobe analyses (wt.%) of allanite and chevkinite from peralkaline (PA) A-type granites, southeast coastal area of China.

	Allanite				Chevkinite					
	Qingtian				Qingtian		Taohuadao		Kuiqi	
	1	2	3	4	5	6	7	8	9	10
P_2O_5	0.01	0.04	–	0.08	0.06	0.04	0.01	–	0.05	0.07
SiO_2	30.82	30.46	33.06	32.95	21.00	19.67	19.87	20.29	21.88	21.20
TiO_2	2.00	3.00	1.59	0.85	18.41	18.38	9.77	10.13	18.46	18.00
ThO_2	0.16	0.16	0.06	0.05	0.82	0.75	0.14	0.23	1.62	1.85
UO_2	–	–	–	0.02	0.07	–	–	–	–	0.07
Al_2O_3	6.49	4.18	14.32	18.25	0.30	0.21	0.45	0.39	2.60	2.68
Y_2O_3	0.97	2.13	2.40	3.72	0.53	0.49	2.78	3.01	0.05	0.08
La_2O_3	7.24	4.95	3.77	2.49	12.15	11.86	10.25	9.93	17.44	16.27
Ce_2O_3	11.83	11.06	8.99	6.58	20.35	20.40	24.11	23.82	19.83	20.19
Pr_2O_3	1.16	0.98	0.77	0.69	1.73	1.95	2.39	2.32	1.02	1.04
Nd_2O_3	3.22	3.89	2.38	2.02	7.97	7.54	9.17	8.50	1.54	2.02
Sm_2O_3	0.55	1.05	0.66	0.84	0.32	0.78	1.58	1.49	–	0.32
Gd_2O_3	0.25	0.40	0.90	1.17	0.80	0.74	0.94	1.06	0.13	–
Dy_2O_3	0.06	0.22	0.58	0.55	0.16	0.18	0.42	0.54	0.21	0.14
Ho_2O_3	–	–	–	0.11	0.05	0.14	–	–	–	–
Er_2O_3	0.26	0.26	0.26	0.57	–	0.03	0.31	0.40	0.21	0.05
Tm_2O_3	0.25	–	0.09	–	–	0.10	0.13	0.10	0.03	0.14
Yb_2O_3	0.10	0.20	0.17	0.28	0.37	0.12	0.89	0.91	0.12	0.27
Lu_2O_3	–	0.07	0.21	0.06	0.06	0.03	0.23	0.35	0.11	0.13
MgO	0.13	0.30	0.15	0.15	–	–	–	–	0.54	0.04
CaO	9.27	9.19	11.00	11.60	2.95	3.13	1.51	1.32	5.65	5.37
MnO	0.96	0.55	0.70	0.94	–	–	1.52	1.61	-	–
FeO^*/FeO_T	13.96	14.76	13.02	10.96	10.57	10.51	10.37	9.52	7.52	7.69
Fe_2O_3*	7.65	9.46	4.44	4.54						
Total	97.32	97.30	99.52	99.50	98.66	97.05	96.85	95.92	99.00	97.61
P (a.p.f.u.)	0.001	0.004	0.000	0.006	0.011	0.007	0.002		0.008	0.011
Si	3.163	3.243	3.113	3.010	4.311	4.151	4.531	4.625	4.281	4.249
Ti	0.154	0.240	0.113	0.058	2.843	2.918	1.677	1.737	2.716	2.712
Th	0.004	0.004	0.001	0.001	0.038	0.036	0.007	0.012	0.072	0.084
U	0.000			0.000	0.003					0.003
Al	0.785	0.524	1.590	1.965	0.073	0.053	0.121	0.104	0.600	0.633
Y	0.053	0.121	0.120	0.181	0.058	0.055	0.337	0.365	0.005	0.008
La	0.274	0.194	0.131	0.084	0.920	0.923	0.862	0.835	1.258	1.203
Ce	0.445	0.431	0.310	0.220	1.530	1.576	2.014	1.989	1.420	1.481
Pr	0.043	0.038	0.026	0.023	0.129	0.150	0.198	0.193	0.073	0.076
Nd	0.118	0.148	0.080	0.066	0.585	0.568	0.747	0.692	0.107	0.145
Sm	0.020	0.038	0.021	0.027	0.023	0.057	0.124	0.117		0.022
Gd	0.008	0.014	0.028	0.035	0.054	0.052	0.071	0.080	0.008	0.000
Dy	0.002	0.008	0.017	0.016	0.010	0.012	0.031	0.039	0.013	0.009
Ho	0.000			0.003	0.003	0.010				
Er	0.008	0.009	0.008	0.016		0.002	0.022	0.028	0.013	0.003
Tm	0.008		0.003			0.006	0.009	0.007	0.002	0.009
Yb	0.003	0.007	0.005	0.008	0.023	0.008	0.062	0.063	0.007	0.017
Lu	0.000	0.002	0.006	0.002	0.004	0.002	0.016	0.024	0.006	0.008
Mg	0.019	0.047	0.021	0.020					0.157	0.011
Ca	1.019	1.048	1.110	1.135	0.649	0.707	0.368	0.322	1.185	1.153
Mn	0.083	0.050	0.056	0.072	0.000	0.000	0.294	0.310		
Fe^{2+}	1.198	2.072	1.340	1.149	1.814	1.854	1.979	1.816	1.230	1.289
Fe^{3+}	0.591	0.736	0.311	0.308						
Σ	8.000	8.000	8.000	7.999	13.082	13.147	13.474	13.358	13.163	13.127

Structural formulae are calculated based on O = 12.5 and 22 atoms per formula unit (a.p.f.u.) for allanite and chevkinite, respectively.

*: The Fe^{2+}/Fe^{3+} ratio was calculated on the basis of 25 positive charges for allanite

–: below detection limit. n.a.: not analysed.

TABLE 4. Electron microprobe analyses (wt.%) of titanite from A-type granites, southeast coastal area of China.

	Peralkaline (PA) A-type						Aluminous (AA) A-type			
	THD	Kuiqi			Laoshan[a]		Putuo.		Xincun[b]	
	1	2	3	4	5	6	7	8	9	10
Nb_2O_5	0.27	0.22	0.35	0.15	2.23	2.22	0.27	0.23	0.10	0.31
Ta_2O_5	–	0.02	0.11	–	0.20	0.15	–	–	–	0.06
SiO_2	29.33	25.95	25.83	29.58	29.58	29.87	27.66	28.27	28.59	29.76
TiO_2	36.46	35.58	35.83	33.57	33.13	33.14	33.00	29.22	30.03	32.35
ZrO_2	0.24	0.09	0.06	0.11	0.16	0.19	–	–	0.03	0.00
HfO_2	–	–	0.03	–	0.03	0.09	0.01	–	0.00	n.a.
ThO_2	0.06	0.01	–	0.06	–	0.01	–	0.01	–	n.a.
UO_2	–	–	–	0.00	–	–	–	–	–	n.a.
Al_2O_3	1.51	1.30	1.91	1.70	0.02	–	8.51	9.01	9.41	3.36
Y_2O_3	0.29	1.29	1.34	0.48	1.52	1.79	0.09	0.07	0.01	n.a.
La_2O_3	0.32	0.37	0.32	0.37	0.11	0.16	–	0.00	0.01	n.a.
Ce_2O_3	1.11	1.24	1.53	1.37	1.68	1.70	0.11	0.00	0.01	n.a.
Nd_2O_3	0.41	0.24	0.39	0.42	n.a.	n.a.	–	0.01	0.04	0.00
CaO	26.63	24.69	23.97	26.53	23.08	23.04	27.67	27.97	27.72	29.23
MgO	0.09	0.04	–	0.02	0.05	0.02	0.04	0.04	0.04	0.00
MnO	0.13	0.59	0.63	0.09	1.26	1.41	0.14	0.29	0.10	0.04
FeO	2.05	3.36	3.19	2.33	5.07	4.93	0.74	1.20	1.11	1.09
Na_2O	–	0.10	0.03	–	0.33	0.36	–	–	0.02	0.01
Total	98.90	95.10	95.50	96.78	98.45	99.08	98.24	96.30	97.22	96.21
Nb (a.p.f.u.)	0.004	0.004	0.006	0.002	0.035	0.034	0.004	0.004		0.005
Ta			0.001		0.002	0.001				0.001
Si	0.988	0.920	0.921	1.016	1.018	1.024	0.942	0.977	0.979	1.009
Ti	0.924	0.949	0.960	0.867	0.858	0.854	0.845	0.759	0.774	0.825
Zr	0.004	0.002	0.001	0.002	0.003	0.003				
Hf						0.001				
Th				0.001						
U										
Al	0.030	0.027	0.040	0.034			0.171	0.183	0.190	0.067
Y	0.005	0.024	0.025	0.009	0.028	0.033	0.002	0.001		
La	0.004	0.005	0.004	0.005	0.001	0.002				
Ce	0.014	0.016	0.020	0.017	0.021	0.021	0.001			
Nd	0.002	0.002	0.002	0.003						
Ca	0.961	0.938	0.915	0.976	0.851	0.846	1.010	1.036	1.018	1.062
Mg	0.004	0.002		0.001	0.003	0.001	0.002	0.002	0.002	
Mn	0.001	0.006	0.006	0.001	0.012	0.014	0.001	0.003	0.001	
Fe	0.058	0.100	0.095	0.067	0.146	0.141	0.021	0.035	0.032	0.031
Na		0.007	0.002		0.022	0.024			0.002	0.001

THD: Taohuadao granite; Structural formula calculated based on Σ cations = 3.
–: below detection limit
n.a.: not analysed
[a] from Wang *et al.* (2001)
[b] from Zhou and Wu (1994)

from PA granites contains 3.4–10.1 wt.% TiO_2, and is thus titanian magnetite. In contrast, abundant magnetite in the Putuoshan, Xincun and Wushan granites of the AA subgroup is distinctly poorer in Ti, ranging from 0.7 to 1.0 wt.% TiO_2.

Ilmenite

Ilmenite occurs in the two subgroups of the A-type granites. However, the chemical composition, especially the MnO and ZnO contents, are quite different (Table 7, Fig. 7*b*). The MnO

TABLE 5. Electron microprobe analyses (wt.%) of pyrochlore from the Kuiqi peralkaline (PA) A-type granites, southeast coastal area of China.

	Grain 1			Grain 2			Grain 3		
	Pyc-I	Pyc-II	Pyc-III	Pyc-I	Pyc-II	Pyc-III	Pyc-I	Pyc-II	Pyc-III
Na_2O	4.28	0.16	0.10	4.43	–	0.04	4.51	0.02	0.06
CaO	1.68	0.27	0.57	1.95	0.29	0.29	1.67	0.20	0.23
PbO	3.05	17.43	44.65	3.13	18.13	47.96	2.21	19.91	57.33
ThO_2	1.18	1.12	1.45	1.01	0.83	0.40	1.06	0.80	0.38
UO_2	12.22	11.09	5.70	11.88	9.91	4.82	14.02	11.11	2.07
La_2O_3	2.21	2.24	1.04	2.47	1.83	0.21	2.26	2.29	–
Ce_2O_3	7.08	6.80	3.17	6.49	5.48	1.36	6.67	6.47	0.44
Nb_2O_5	50.77	48.54	29.05	50.11	43.64	32.62	51.21	42.96	30.46
Ta_2O_5	1.71	0.96	1.14	2.50	1.23	1.40	1.43	1.05	0.29
TiO_2	10.25	8.90	5.71	10.14	8.63	4.85	11.09	8.60	6.07
F	2.52	0.69	0.66	2.28	0.75	0.44	3.04	0.53	0.55
F=O	1.06	0.29	0.28	0.96	0.32	0.18	1.28	0.23	0.23
Total	95.88	97.92	92.96	95.43	90.40	94.21	97.89	93.71	97.65
Na (a.p.f.u.)	0.533	0.022	0.022	0.555		0.009	0.549	0.003	0.012
Ca	0.116	0.020	0.069	0.135	0.023	0.033	0.113	0.016	0.027
Pb	0.053	0.325	1.355	0.054	0.368	1.375	0.037	0.409	1.676
La	0.052	0.057	0.043	0.059	0.051	0.008	0.052	0.064	
Ce	0.167	0.172	0.131	0.153	0.151	0.053	0.153	0.181	0.017
Th	0.017	0.018	0.037	0.015	0.014	0.010	0.015	0.014	0.009
U	0.175	0.171	0.143	0.171	0.166	0.114	0.196	0.189	0.050
Nb	1.475	1.519	1.481	1.464	1.486	1.571	1.453	1.484	1.496
Ta	0.030	0.018	0.035	0.044	0.025	0.041	0.024	0.022	0.009
Ti	0.495	0.463	0.484	0.493	0.489	0.388	0.523	0.494	0.496
B site	2.000	2.000	2.000	2.000	2.000	2.000	2.000	2.000	2.000
F	0.512	0.151	0.234	0.465	0.179	0.148	0.604	0.129	0.188

Structural formula calculated based on Nb+Ta+Ti = 2
–: below detection limit;
n.a.: not analysed

content in ilmenite from the PA granites varies significantly, from 2.4 to 20.1 wt.%, with an average of 15 wt.%, and a few grains contain up to 37.4 wt.% MnO. Nb-rich ilmenite in the Laoshan PA granite and Zn-rich ilmenite in the Kuiqi PA granite have been reported previously by Wang *et al.* (2001) and Suwa *et al.* (1987), respectively. In contrast, the amount of Mn in ilmenite from the AA granites ranges from 27 to 41 wt.% with an average of 35 wt.% MnO, which is 20 wt.% greater than the average MnO content in ilmenite in the PA granite. Concentrations of Nb, Ta and Zn are small and frequently <1 wt.%. Most ilmenites in this subgroup are pyrophanite.

Rutile

The phase commonly appears as part of the complex association of Ti-Fe oxide minerals within the Wushan aluminous granite, whereas it is sporadic or absent in PA granite.

Discussion

The stability of accessory minerals is controlled by a range of parameters, notably temperature, melt composition and oxygen fugacity (Cuney and Friedrich, 1987). As a consequence, the textural records of growth, chemical zoning and dissolution of such phases provide indications of

TABLE 6. Electron microprobe analyses (wt.%) of monazite from A-type granites, southeast coastal area of China.

	Aluminous (AA) A-type				Peralkaline (PA) A-type			
	1	2	3	4	5	6	7	8
P_2O_5 (wt.%)	28.56	21.54	27.25	22.77	30.77	29.43	29.19	30.39
SiO_2	1.46	6.52	0.66	5.26	–	–	–	–
ThO_2	8.19	25.45	11.03	20.47	0.69	1.00	0.27	0.26
UO_2	0.20	0.24	0.21	0.31	0.00	–	–	–
Y_2O_3	2.03	0.59	1.77	0.74	0.10	0.01	0.39	0.19
La_2O_3	14.67	13.18	13.82	13.51	15.70	13.52	21.80	23.67
Ce_2O_3	29.67	22.48	26.12	24.05	39.99	40.61	35.55	37.43
Pr_2O_3	2.80	2.27	2.26	2.57	3.28	4.01	2.48	2.50
Nd_2O_3	6.34	4.86	9.81	4.97	6.35	8.73	7.96	3.26
Sm_2O_3	2.17	1.03	1.69	0.99	1.67	0.11	0.70	0.31
Gd_2O_3	1.37	0.43	1.17	0.64	0.26	0.16	0.26	–
Tb_2O_3	0.02	0.24	0.09	–	0.11	n.a.	0.04	0.07
Dy_2O_3	0.45	0.05	0.23	0.01	–	0.22	0.12	0.02
Ho_2O_3	–	0.05	0.01	0.07	0.15	0.29	0.03	–
Er_2O_3	0.17	0.30	0.33	–	0.15	–	–	0.19
Tm_2O_3	0.26	0.12	–	0.25	0.07	0.32	–	–
Yb_2O_3	0.07	0.06	0.20	–	–	–	–	–
Lu_2O_3	0.10	0.05	0.06	–	0.17	–	–	–
MgO	–	–	–	–	–	–	–	–
CaO	0.25	0.18	1.37	0.22	0.03	0.01	0.22	0.12
F	0.83	0.64	0.69	0.70	1.01	n.a.	1.27	1.63
O=F	0.35	0.27	0.29	0.30	0.43		0.53	0.68
Total	99.26	100.00	98.46	97.23	100.06	98.41	99.72	99.34
P (a.p.f.u.)	0.936	0.747	0.927	0.795	0.976	0.939	0.948	0.963
Si	0.057	0.267	0.027	0.217				
Th	0.072	0.237	0.101	0.192	0.006	0.009	0.002	0.002
U	0.002	0.002	0.002	0.003	0.000			
Y	0.042	0.013	0.038	0.016	0.002		0.008	0.004
La	0.209	0.199	0.205	0.206	0.217	0.188	0.309	0.327
Ce	0.421	0.337	0.384	0.363	0.549	0.561	0.499	0.513
Pr	0.040	0.034	0.033	0.039	0.045	0.055	0.035	0.034
Nd	0.088	0.071	0.141	0.073	0.085	0.118	0.109	0.044
Sm	0.029	0.015	0.023	0.014	0.022	0.001	0.009	0.004
Gd	0.018	0.006	0.016	0.009	0.003	0.002	0.003	
Tb	0.000	0.003	0.001		0.001			0.001
Dy	0.006	0.001	0.003	0.000		0.003	0.001	0.000
Ho		0.001	0.000	0.001	0.002	0.004	0.000	
Er	0.002	0.004	0.004		0.002			0.002
Tm	0.003	0.002		0.003	0.001	0.004		
Yb	0.001	0.001	0.002					
Lu	0.001	0.001	0.001		0.002			
Mg								
Ca	0.010	0.008	0.059	0.010	0.001		0.009	0.005
F	0.101	0.083	0.088	0.092	0.120		0.154	0.192

Structural formula calculated based on O = 4
–: below detection limit
n.a.: not analysed

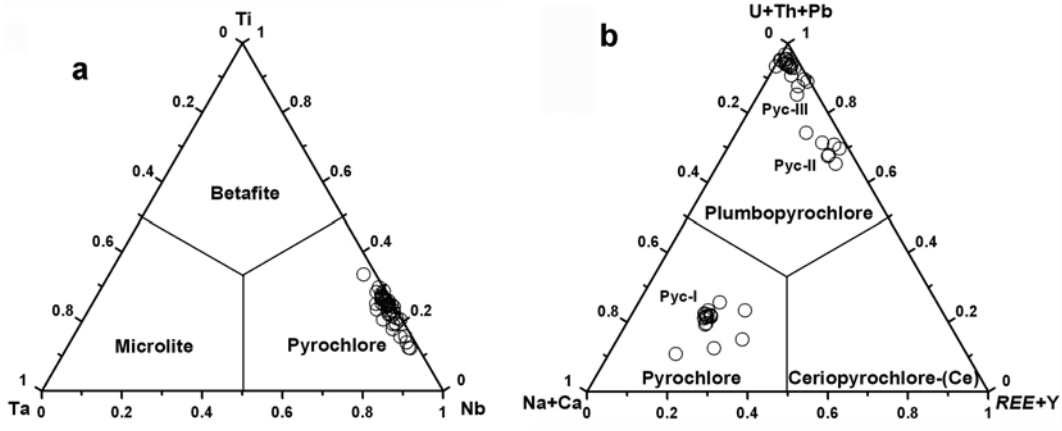

FIG. 6. Classification diagrams for pyrochlore analyses. (*a*) Classification on the atomic proportions of Nb, Ta and Ti in pyrochlore from the Kuiqi and Laoshan PA subgroup A-type granites. (*b*) Classification according to *A*-site cations. Figure 5*d* shows the textural relations between the three pyrochlore populations Pyc-I, Pyc-II and Pyc−III.

the magmatic and post-magmatic history of rocks (Robinson and Miller, 1999; Dini *et al.*, 2004).

Comparison of accessory minerals in PA and AA subgroups

In Table 8 we summarize the relative abundance of accessory minerals in the two subgroups of A-type granites in southeastern coastal China. In the PA granites, zircon occurs as the predominant accessory mineral. It has a diagnostic internal texture and composition; primary magmatic Th-rich zircon is overgrown by thorite-containing Th-poor zircon (Xie *et al.*, 2005). The *REE* minerals in this granite subgroup include allanite-(Ce), chevkinite-(Ce), titanite and pyrochlore. Ti-Fe oxides consist of titanian magnetite and Mn-bearing ilmenite. In the AA granite subgroup, zircon is subhedral to euhedral with weakly developed zoning and has a very low Th content, but relatively high U content. The *REE* minerals are dominated by Th-rich monazite or xenotime rather than *REE*-bearing silicates. Ti-poor magnetite, pyrophanite and rutile are the main Ti-Fe oxides.

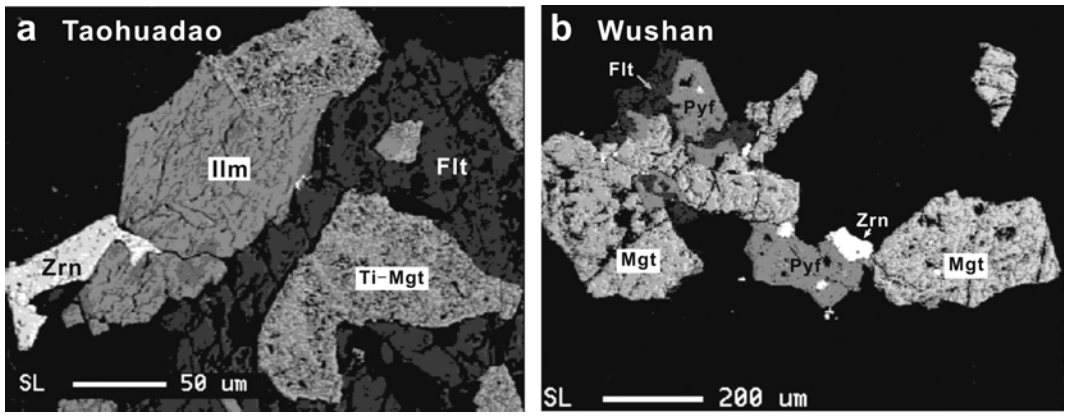

FIG. 7. Backscattered electron images of coexisting Fe-Ti oxide minerals in: (*a*) Taohuadao peralkaline (PA) A-type granite; and (*b*) the Wushan aluminous (AA) A-type granite. Mineral abbreviations: Ilm = ilmenite; Mgt = magnetite; Ti-Mgt = titanomagnetite; Zrn = zircon; Pyf = pyrophanite; Flt = fluorite.

TABLE 7. Representative electron microprobe analyses (wt.%) of Fe-Ti oxide minerals from A-type granites, southeast coastal area of China.

	Peralkaline (PA) A-type granites											
	1		2		3		4		5		6	
	Ilm	Mgt	Ilm	Mgt	Ilm	Mgt	Ilm	Mgt	Ilm	Mgt	Ilm	Mgt
Nb_2O_5	0.73	0.09	0.19	–	–	–	0.05	–	0.39	–	0.13	0.03
Ta_2O_5	0.02	0.01	–	–	–	–	–	–	0.20	0.41	0.03	0.08
FeO*	34.32	38.20	33.11	44.06	23.77	37.65	14.54	31.83	22.69	37.61	6.57	30.41
Fe_2O_3*	7.08	48.32	5.21	40.64	6.60	44.17	3.05	63.24	2.64	45.93	5.27	55.63
TiO_2	47.26	10.12	48.73	14.69	49.25	12.32	50.30	2.92	49.72	9.95	49.64	4.72
SnO_2	0.02	0.01	–	–	–	–	–	–	–	–	–	–
MgO	0.01	–	–	0.01	0.01	–	0.0	–	–	–	–	0.02
MnO	7.98	2.10	10.56	0.95	20.11	4.71	29.72	1.73	21.46	1.62	37.37	3.53
ZnO	0.09	0.05	0.02	0.03	0.15	0.11	0.68	0.13	0.32	0.10	0.26	–
Total	97.50	98.92	97.81	100.38	99.89	98.96	98.33	99.86	97.43	95.61	99.26	94.42
$\log_{10}f_{O_2}$	−14.86		−15.42		−13.12		−17.47		−18.80		−11.96	
T	769		774		840		656		668		817	
ΔFMQ	0.543		0.220		0.682		0.830		0.900		2.340	

	Aluminous (AA) A-type granites											
	7		8		9		10		11		12	
	Ilm	Mgt	Ilm	Mgt	Ilm	Mgt	Ilm	Mgt	Ilm	Mgt	Ilm	Mgt
Nb_2O_5	0.01	–	0.23	–	0.09	0.13	0.19	–	0.10	0.02	0.20	0.12
Ta_2O_5	0.13	–	0.23	–	0.11	0.25	–	–	–	0.19	0.35	0.05
FeO*	4.27	30.41	8.00	29.88	7.36	31.58	14.10	31.73	16.06	29.86	13.36	30.88
Fe_2O_3*	4.52	66.37	3.00	66.79	8.15	66.97	5.01	67.71	5.95	65.39	5.07	65.85
TiO_2	51.17	1.04	49.97	0.84	48.17	0.62	50.41	0.81	48.60	0.94	49.63	1.04
SnO_2	0.01	–	0.05	–	0.02	–	0.0	–	–	–	–	–
MgO	–	0.00	0.02	–	0.01	–	0.01	0.01	–	0.02	–	–
MnO	41.12	1.64	36.44	2.01	35.42	0.46	30.81	0.53	27.15	1.45	30.74	0.96
ZnO	0.10	0.10	–	0.09	0.07	0.20	0.01	0.11	0.16	0.48	0.15	0.41
Total	101.33	99.57	97.94	99.61	99.40	100.23	100.57	100.89	98.03	98.35	99.49	99.30
$\log_{10}f_{O_2}$	−12.80		−14.89		−13.11		−15.07		−14.89		−14.76	
T	715		658		684		652		663		669	
ΔFMQ	5.296		3.213		4.388		3.334		3.209		3.337	

1−3: Qingtian; 4−6: Taohuadao
−: below the detection limit (Nb, Ta, Mg, Sn: 100 ppm), Ilm: ilmenite; Mgt: magnetite
*: FeO/Fe_2O_3 ratio calculated by assuming ideal stoichiometry for magnetite and ilmenite
$\log_{10}f_{O_2}$ and T calculated from coexisting ilmenite and magnetite (after Carmichael, 1967; Lindsley and Spencer, 1982; Lepage, 2003)
ΔFMQ calculated after Frost (1991)

There exists a limited number of studies of accessory minerals in A-type granites elsewhere in the world. Bonin *et al.* (1998) described an accessory mineral assemblage in the peralkaline granite from the Taourirt suite of Hoggar, Algeria, comprising zircon, allanite, chevkinite, ilmenite and magnetite. In that study, these accessory minerals were also described for the typical peralkaline arfvedsonite-aegirine granite from the Saibro intrusive suite of southern Brazil. In comparison, the peraluminous anorogenic Gross Spitzkoppe granite of central western Namibia, contains an assemblage of topaz, fluorite, magnetite, zircon, monazite and thorite (Frindt *et al.*, 2004). Studies by Förster (1998*a,b*) found the *REE* phosphates, monazite-(Ce), Ca-rich monazite-(Ce) [formerly cheralite-(Ce)], and xenotime in Li-mica-bearing peraluminous

TABLE 8. Summary of accessory mineral assemblages from of A-type granite subgroups, southeast coastal area of China.

	Peralkaline (PA) A-type				Aluminous (AA) A-type			
	Laoshan	Taohuadao	Qingtian	Kuiqi	Suzhou	Putuoshan	Xincun	Wushan
Th-rich zircon	++	+++	++	++	–	–	–	–
Th-poor zircon	++[1]	++[1]	+[1]	+[1]	++[2]	++[2]	+[2]	+[2]
Thorite	+	+	+	–	+	+	+	+
Magnetite	+++	+++	+++	+++	+++	+++	+++	+++
Ilmenite	+	++	++	+	+	–	–	+
Pyrophanite	+	+	+	–	+	++	++	+
Rutile	–	–	–	–	+	+	–	+
Allanite	+	+	++	++	–	–	–	–
Chevkinite	+	++	+++	+	–	+	–	–
Titanite	++	+	–	+	+[3]	++[3]	–	–
Pyrochlore	++	+	+	++	–	–	–	–
Monazite-(Ce)	+	+	–	+	++[4]	++[4]	++[4]	++[4]
Fluocerite	+++	+++	+++	+++	++	++	++	+
Fluorite	+++	+++	++	+++	+	+	++	+
Apatite	+	+	++	+	++	+++	++	++
Bastnäsite-(Ce)	++	++	+	++	++	++	+	++
Xenotime-(Y)	–	–	–	–	–	+	+	–

–: rare or absent; +: relatively abundant; ++: more abundant; +++: most frequent.
[1] thorite-containing Th-poor zircon; [2]inclusion-free Th-poor zircon; [3]Al-rich titanite; [4]Th-rich monazite-(Ce).

A-type granite of eastern Germany. Therefore, the assemblages and compositional features of accessory minerals in the granites of this present study may well represent universal signatures of these types of granites.

Magmatic and hydrothermal zircon: metasomatic breakdown of Th-rich zircon in peralkaline granites

The solubility of Th in zircon has been determined experimentally to be ~4 ± 2 mol.% (or 5.5 ± 2.5 wt.% ThO_2; Mumpton and Roy, 1961). However, experimental runs under anhydrous conditions in that study are different from the complex environment in which natural thorian zircon solid solutions have formed. In fact, higher Th abundances can be found in natural zircon, such as 10.6 wt.% ThO_2 in a metamict zircon from the Ebisu mine, Japan (Farges and Calas, 1991). The most Th-rich zircon, containing in 42.3 wt.% was recently recorded from the Feddan alkali-feldspar granite, Jordan (Förster, 2006). In particular, high-Th contents are usually characteristic of zircon that form from a peralkaline magma, e.g. 9.4 wt.% ThO_2 in zircon from the Sierra Blanca peralkaline rhyolite, Texas (Rubin *et al.*, 1989), as well as ~11 wt.% reported in zircon from peralkaline A-type granites in this study. It is noteworthy that magmatic zircon without thorite inclusions is probably an important host of thorium in peralkaline granite. This feature of zircon from peralkaline A-type granites may reflect a high concentration of thorium inherited from the magma source region, a high-temperature and peralkaline environment, but this is speculative and requires further work.

Moreover, as shown in this study, peralkaline southeastern Chinese granites are also characterized by overgrowths or mantles of porous Th-poor zircon with abundant inclusions of thorite on cores of primary, magmatic Th-rich zircon. This texture, in combination with amoeboid zircon penetrating adjacent Ti-Fe oxides, resembles the textures of zircon of hydrothermal origin. Hydrothermal zircon is crystallized from or altered by an aqueous fluid (Hoskin, 2005), and has been described for peralkaline environments by Rubin *et al.* (1989), Hoskin and Schaltegger (2003), and Förster (2006). Magmatic Th-rich zircon may be recrystallized to a hydrothermally-equilibrated secondary zircon by late-stage metasomatism in peralkaline granites (Wang *et al.*, 2001). This process is probably responsible for producing the zircon mantles described in this

study. In contrast, the well developed zoned zircon crystals in the aluminous subgroup granites in our study do not show comparable compositions and textures. We infer that the composition of the fluid that may have interacted with these zircons during late-stage crystallization was different to the late-stage fluid in the peralkaline granites. Relevant experimental work to support this inference has not yet been conducted.

REE silicates vs. REE phosphates: influence of melt composition

The *REE* minerals in the two distinct subgroups of granites are distinctive. The stabilities of *REE*-silicates and phosphates are controlled by magma composition, in particular magmatic peralkalinity or peraluminosity. The *REE*-bearing silicates chevkinite-(Ce), allanite-(Ce) and titanite are present in PA granites. Chevkinite is widely reported in peralkaline igneous rocks worldwide. Troll *et al.* (2003) demonstrated that chevkinite acts as a refractory mineral during partial melting and assimilation of alkaline rock and thus inhibits release of La, Ce, Nb, Y and Zr into the melt. Allanite also has low solubility during partial melting and together with chevkinite occurs in alkaline magmas (Robinson and Miller, 1999). These authors suggest that magma peralkalinity strongly controlled the stability relations of monazite-(Ce), allanite-(Ce), and fluorapatite in magma producing the Aztec Wash pluton, Nevada, USA.

The *REE* phosphates, principally monazite-group minerals and less importantly xenotime, typify AA granites. The AA granites have greater aluminosity (mainly ASI > 1.0) than peralkaline granites (A/NK, by definition). Experimental results indicate that *REE* phosphates are sensitive to melt aluminosity. Rapp and Watson (1986) demonstrated that monazite solubility in monazite-saturated melts decreases as peraluminosity increases (Fig. 8). Similarly, Watson (1980) and Montel (1985) show that the solubility of both apatite and monazite increase markedly with increasing peralkalinity. The low solubility of phosphate phases thereby depletes the magma in P and *LREE* and causes the late-stage formation of other *REE* accessory minerals such as xenotime and bastnäsite (Cuney and Friedrich, 1987). However, the mineral association monazite + thorite may form instead of allanite in a aluminous melt with lower Ca activity (Fig. 8). Therefore, the nature of AA granite magma being of greater aluminosity and lower Ca activity favours the saturation of *REE* phosphates.

Crystallization parameters: temperature and oxygen fugacity

The temperature of crystallization of accessory minerals can be estimated using Fe-Ti oxide mineral thermometry and zircon-saturation thermometry (Carmichael, 1967; Lepage, 2003; Watson and Harrison, 1983). Making use of coexisting Ti-Fe oxide minerals, we calculated temperatures for PA and AA granites in the range of 840−656ºC and 700−650ºC, respectively (Table 7), using the spreadsheet template of Lepage (2003). Using the zircon-saturation thermometer of Watson and Harrison (1983) and whole-rock compositional data for rock samples used in this study (data from: Peng and Dong, 1991; Wang *et al.*, 1996; Zhao *et al.*, 1997; Qiu *et al.*, 1996, 2004), temperatures of 750−930ºC for PA granites and 720−820ºC for AA granites were calculated. Despite the range of calculated temperatures obtained by the two thermometery methods, the calculated temperature of crystallization of PA granites is systematically greater than that for AA granites.

For the PA granites, the relative oxygen fugacity at crystallization was calculated using the above-calculated temperatures and the methodology of Lindsley and Spencer (1982), and is found to vary between 0.2 and 2.3 log units above the FMQ buffer. The calculated oxygen fugacity

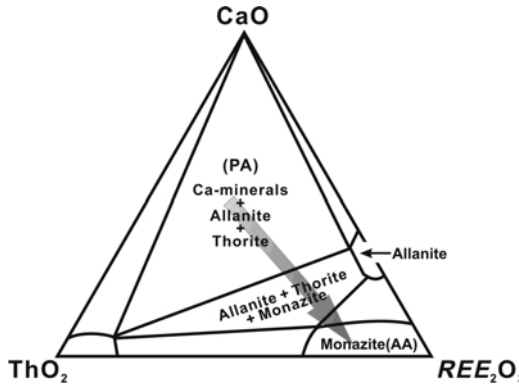

FIG. 8. Phase assemblages in the system CaO-ThO_2-REE_2O_3 in granitoids (modified after Cuney and Friedrich, 1987). The arrow indicates increasing ASI of the granitic magma. 'PA' and 'AA' indicate the mineral assemblages of the PA and AA granite subgroups, respectively.

for AA granite crystallization is from FMQ +3.2 to FMQ +5.3 (Table 7 and Fig. 9). For the PA granite subgroup, these calculated oxygen fugacity values are interpreted to represent conditions extant at magmatic crystallization because ilmenite and magnetite are euhedral and appear not to have suffered post-crystallization exsolution or hydrothermal alteration. Marks *et al.* (2003) suggested that in most peralkaline rock-types, arfvedsonite and aegirine occur as late-magmatic phases and indicate an increase in oxygen fugacity. The relatively oxidized crystallization conditions inferred for the PA granites may be thus indicated by the occurrence of these two minerals in the granites.

It appears that the AA granites developed under highly oxidizing conditions (FMQ +3.2−5.3). In AA granites, rutile and pyrophanite are usually present whereas in the PA granites, titanian magnetite occurs together with rare rutile. Experimental results show that the incorporation of the pyrophanite molecule in ilmenite is favoured by more oxidizing conditions (Czamanske and Wones, 1973) as indicated by the reaction:

$$8(Fe_{0.75}Mn_{0.25})TiO_3 + O_2 \rightarrow 4(Fe_{0.5}Mn_{0.5})TiO_3 + 2Fe_2O_3 + 4TiO_2 \quad (1)$$

On the basis of our results, we infer that the PA granites crystallized at higher temperature and under conditions of lower oxidation than did the AA granites of the southeast coastal area of China. These temperature and oxidation differences may be explained if it is considered that the peralkaline (PA) magmas crystallized at greater pressures, probably in an extensional environment. The depth of A-type silicic magma generation is a matter of debate (Litvinovsky *et al.*, 2002) and it is likely that A-type granites are generated in different tectonic settings with variable mantle and crustal inputs (Wu *et al.*, 2002). Recently, Qiu *et al.* (2004) concluded that the PA granites of the southeast coastal area of China formed as a result of the combined effects of fractionation and a deeper mantle source than that for AA granite magmas. We suggest that deep-level generation of magma implies a higher temperature and an upper mantle source for the PA granite magmas, and we show that they crystallized in a less oxidizing environment than the AA granite magmas of the southeast coastal area of China.

Conclusions

A-type granites represent a volumetrically important but highly variable group of rocks worldwide. Few studies have focused on the accessory mineral assemblages of A-type granites. For this study, the coeval peralkaline (PA) and aluminous (AA) A-type granite subgroups of the southeastern coastal area of China have been studied. The differing bulk compositions and crystallization conditions of these granite subgroups are reflected in their

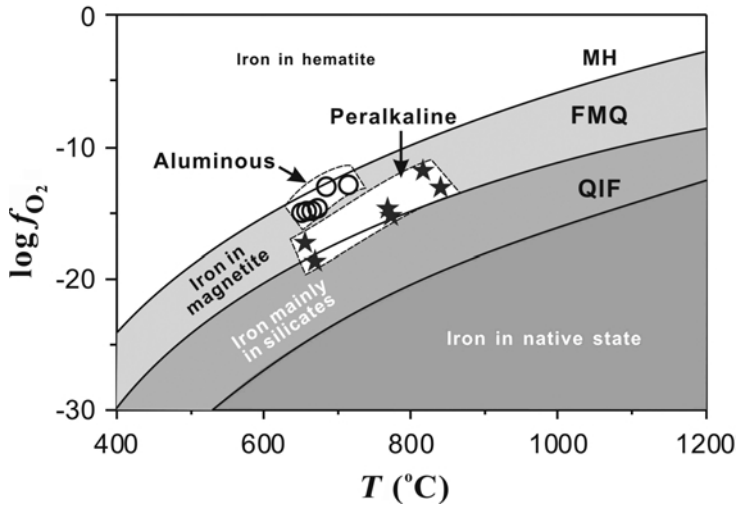

FIG. 9. Plot of $\log f_{O_2}$ *vs.* T showing the calculated crystallization conditions for peralkaline (PA) and aluminous (AA) A-type granites from southeastern coastal China (modified after Frost, 1991).

distinctive accessory mineral assemblages. Intergrowths of Th-rich and porous Th-poor zircon, *REE* silicates [allanite-(Ce), chevkinite-(Ce), titanite], titanian magnetite and ilmenite occur in PA granites, whereas euhedral Th-poor zircon without inclusions, *REE* phosphates [monazite-(Ce), xenotime-(Y)], magnetite and pyrophanite occur in AA granites. The occurrence of these accessory mineral assemblages are essentially controlled by melt composition, temperature, and oxygen fugacity. Peralkaline melts favour the formation of *REE* silicates, whereas the relatively higher ASI of AA granite melts promotes the precipitation of *REE* phosphates. The peralkaline (PA) granites of southeast coastal China are inferred to have crystallized at greater temperatures (by 50–100ºC) than those of aluminous (AA) granites and under less oxidizing conditions. The two granite subgroups are coeval, but are interpreted to have derived from different lithospheric sources. The PA subgroup magmas were produced at greater depths and presumably have a greater proportion of mantle material. While our dataset is sufficient to highlight first-order processes and differences in granite petrogenesis, we recognize that our present dataset will benefit greatly from ongoing studies on the significance and nature of intrusive rocks of southeast coastal China.

Acknowledgements

The authors express thank Associate Editor, P.W.O. Hoskin, and H.-J. Förster and R.F. Martin for constructive reviews and suggestions which greatly improved the manuscript. We gratefully acknowledge R.H. Grapes for assistance with the English. Financial support was provided by the Natural Science Foundation of China (Grant No. 40221301, 40272036 and 40025209) and the Scientific Research Foundation of Graduate School of Nanjing University.

References

Bonin, B.L., Azzouni-Sekkal, A., Bussy, F. and Ferrag, S. (1998) Alkali-calcic and alkaline post-orogenic (PO) granite magmatism: petrologic constraints and geodynamic settings. *Lithos*, **45**, 45–70.

Carmichael, I.S.E. (1967) The iron-titanium oxides of salic volcanic rocks and their associated ferromagnesian silicates. *Contributions to Mineralogy and Petrology*, **14**, 36–64 .

Casillas, R., Nagy, G., Pantó, G., Bräandle, J. and Fórizs, I. (1995) Occurrence of Th, U, Y, Zr, and REE-bearing accessory minerals in late-Variscan granitic rocks from the Sierra de Guadarrama (Spain). *European Journal of Mineralogy*, **7**, 989–1006.

Cuney, M. and Friedrich, M. (1987) Physicochemical and crystal-chemical controls on accessory mineral paragenesis in granitoids: implications for uranium metallogenesis. *Bulletin de Minéralogie*, **110**, 235–247.

Czamanske, G.K. and Wones, D.R. (1973) Oxidation during magmatic differentiation, Finnmarka Complex, Oslo area, Norway: Part 2, the mafic silicates. *Journal of Petrology*, **14**, 349–380.

Dini, A., Rocchi, S. and Westerman, D.S. (2004) Reaction microtextures of REE-Y-Th-U accessory minerals in the Monte Capanne pluton (Elba Island, Italy): a possible indicator of hybridization processes. *Lithos*, **78**, 101–118.

Farges, F. and Calas, G. (1991) Structural analyses of radiation damage in zircon and thorite: An X-ray absorption spectroscopic study. *American Mineralogist*, **76**, 60–73.

Förster, H.J. (1998*a*) The chemical composition of REE-Y-Th-U-rich accessory minerals in peraluminous granites of the Erzgebirge-Fichtelgebirge region, Germany, Part I: The monazite-(Ce)-brabantite solid solution series. *American Mineralogist*, **83**, 259–272.

Förster, H.J. (1998*b*) The chemical composition of REE-Y-Th-U-rich accessory minerals in peraluminous granites of the Erzgebirge-Fichtelgebirge region, Germany. Part II: Xenotime. *American Mineralogist*, **83**, 1302–1315.

Förster, H.J. (2006) Composition and origin of intermediate solid solutions in the system thorite-xenotime-zircon-coffinite. *Lithos*, **88**, 35–55.

Frindt, S., Haapala, I. and Pakkanen, L. (2004) Anorogenic Gross Spitzkoppe granite stock in central western Namibia: Part I. Petrology and geochemistry. *American Mineralogist*, **89,** 841–856.

Frost, B.R. (1991) Introduction to oxygen fugacity and its petrologic importance. Pp. 1–10 in: *Oxide Minerals: Petrologic and Magnetic Significance* (D. H. Lindsley, editor). Reviews in Mineralogy, **25**, Mineralogical Society of America, Washington, D.C.

Hoskin, P.W.O. (2005) Trace-element composition of hydrothermal zircon and the alteration of Hadean zircon from the Jack Hills, Australia. *Geochimica et Cosmochimica Acta*, **69**, 637–648.

Hoskin, P.W.O and Schaltegger, U. (2003) The composition of zircon and igneous and metamorphic petrogenesis. Pp. 27–62 in: *Zircon* (J.M. Hanchar and P.W.O. Hoskin, editors). Reviews in Mineralogy

& Geochemistry, **53**, Mineralogical Society of America and the Geochemical Society, Washington, D.C.

Jiang, N. (2006) Hydrothermal alteration of chevkinite-(Ce) in the Shuiquangou syenitic intrusion, northern china. *Chemical Geology*, **227**, 100–112.

Lepage, L.D. (2003) ILMAT: an Excel worksheet for ilmenite – magnetite geothermometry and geobarometry. *Computers & Geosciences*, **29**, 673–678.

Lindsley, D.H. and Spencer, K.J. (1982) Fe-Ti oxide geothermometry: Reducing analyses of coexisting Ti-magnetite (Mt) and ilmenite (Ilm). *Abstract AGU Spring Meeting Eos Transactions*, American Geophysical Union, **63**, 471.

Litvinovsky, B.A., Jahn, B.J., Zanbilevich, A.N., Saunders, A., Poulain, S., Kuzmin, D.B., Reichow, M.K. and Titov, A.V. (2002) Petrogenesis of syenite-granite suites from the Bryansky Complex (Transbaikalia, Russia): implications for the origin of A-type granitoid magmas. *Chemical Geology*, **189**, 105–133.

Marks, M., Vennemann, T., Siebel, W. and Markl, G. (2003) Quantification of magmatic and hydrothermal processes in a peralkaline syenite-alkali granite complex unit of the Ilímaussaq Intrusion, South Greenland, as deduced from phase equilibria. *Journal of Petrology*, **44**, 1247–1280.

Martin, H., Bonin, B., Capdevila, R., Jahn, B.M., Lameyre, J. and Wang, Y. (1994) The Kuiqi peralkaline granitic complex (SE China): petrology and geochemistry. *Journal of Petrology*, **35**, 983–1015.

Montel, J.M. (1985) Is monazite guilty? Experimental determination of Ce-monazite solubility in Na_2O, K_2O, SiO_2, Al_2O_3 melts. *Terra Cognita*, **5**, 330.

Mumpton, F.A. and Roy, R. (1961) Hydrothermal stability studies of the zircon-thorite group. *Geochimica et Cosmochimica Acta*, **21**, 217–238.

Pearce, J.A. (1984) Trace element discrimination diagrams for the tectonic interpretation of granitic rocks. *Journal of Petrology*, **25**, 956–983.

Peng, Y.M. and Dong, C.W. (1991) A study on Qingtian alkaline granite, Zhejiang province. *Journal of Nanjing University (Earth Sciences)*, **2**, 138–147 [Chinese with English abstract].

Qiu, J.S., Wang, D.Z., Peng, Y.M. and Zhou, J.C. (1996) Petrology, geochemistry and genesis of Taohuadao alkali granite in Zhoushan, Zhejiang Province. *Journal of Nanjing University (Earth Sciences)*, **32**, 79–89 [Chinese with English abstract].

Qiu, J.S., Wang, D.Z., McInnes, B.I.A., Jiang, S.Y., Wang, R.C. and Kanisawa, S. (2004) Two contrasting A-type granites in the coastal area of Zhejiang and Fujian Province, SE China: geochemical constraints on their petrogenesis. *Transactions of the Royal Society of Edinburgh – Earth Sciences*, **95**, 227–236.

Rapp, R.P. and Watson, E.B. (1986) Monazite solubility and dissolution kinetics: implications for the thorium and light rare earth geochemistry of felsic magmas. *Contributions to Mineralogy and Petrology*, **94**, 304–316.

Robinson, D.M. and Miller, C.F. (1999) Record of magma chamber processes preserved in accessory mineral assemblages, Aztec Wash pluton, Nevada. *American Mineralogist*, **84**, 1346–1353.

Rubin, J.N., Henry, C.D. and Price, J.G. (1989) Hydrothermal zircons and zircon overgrowths, Sierra Blanca Peaks, Texas. *American Mineralogist*, **74**, 865–869.

Suwa, K., Enami, M., Hiraiwa, I. and Yang, T.M. (1987) Zn-Mn ilmenite in the Kuiqi granite from Fuzhou, Fujian Province, East China. *Mineralogy and Petrology*, **36**, 111–120.

Troll, V.R., Sachs, P.M., Schmincke, H.U. and Sumita, M. (2003) The REE-Ti mineral chevkinite in comenditic magmas from Gran Canaria, Spain: a SYXRF-Probe study. *Contributions to Mineralogy and Petrology*, **145**, 730–741.

Tu, G., Zhang, Y. and Zhao, Z. (1982) Preliminary studies on two alkali-rich intrusive belts in south China. Pp. 33–51 in: *Proceeding of the International Symposium held at Nanjing University, Geology of Granites and their Metallogenetic Relations* (K.Q. Xu and G.Z. Tu, editors). Science Press, Beijing.

Wang, D.Z., Zhao, G.T. and Qiu, J.S. (1995) The tectonic constraint on the late Mesozoic A-type granitoids in eastern China. *Geological Journal of China University*, **1**, 13–21 [Chinese with English abstract].

Wang, R.C., Fontan, F., Xu, S.J., Chen, X.M. and Monchoux, P. (1996) Hafnian zircon from the apical part of the Suzhou granite, China. *The Canadian Mineralogist*, **34**, 1001–1010.

Wang, R.C., Zhao, G.T., Chen, X.M., Lu, J.J., Xu, S.J. and Wang, D.Z. (2000) Chemistry of Hf-rich zircons from the Laoshan I- and A- type granites, Eastern China. *Mineralogical Magazine*, **64**, 867–877.

Wang, R.C., Wang, D.Z., Zhao, G.T., Lu, J.J., Chen, X.M. and Xu, S.J. (2001) Accessory mineral record of magma-fluid interaction in the Laoshan I- and A-type granitic complex, eastern China. *Physics and Chemistry of the Earth Part A – Solid Earth and Geodesy*, **26**, 835–849.

Wang, R.C., Fontan, F., Chen, X.M., Hu, H., Liu, C.S., Xu, S.J. and de Parseval, P. (2003) Accessory minerals in the Xihuashan Y-enriched granitic complex, southern China: A record of magmatic and hydrothermal stages of evolution. *The Canadian Mineralogist*, **41**, 727–748.

Watson, E.B. (1980) Apatite and phosphorus in mantle source regions: an experimental study of apatite/melt

equilibria at pressures to 25 kbar. *Earth and Planetary Science Letters*, **51**, 322–335.

Watson, E.B. and Harrison, T.M. (1983) Zircon saturation revisited: temperature and composition effects in a variety of crust magma types. *Earth and Planetary Science Letters*, **64**, 295–304.

Wei, C.S., Zheng, Y.F. and Zhao, Z.F. (2000) Hydrogen and oxygen isotope geochemistry of A-type granites in the continental margins of eastern China. *Tectonophysics*, **328**, 205–227.

Wu, F.Y., Sun, D.Y., Li, H.M., Jahn, B.M. and Wilde, C.S. (2002) A-type granites in northeastern China: age and geochemical constraints on their petrogenesis. *Chemical Geology*, **187**, 143–173.

Xie, L., Wang, R.C., Chen, X.M., Qiu, J.S. and Wang, D.Z. (2005) Th-rich zircon from peralkaline A-type granite: mineralogical features and petrological implications. *Chinese Science Bulletin*, **50**, 809–817.

Zhang, A.C., Wang, R.C., Hu, H., Zhang, H., Zhu, J.C. and Chen, C.M. (2004) Chemical evolution of Nb-Ta oxides and zircon from the Koktokay No. 3 granitic pegmatite, Altai, northwestern China. *Mineralogical Magazine*, **68**, 739–756.

Zhao, G.T., Wang, D.Z. and Cao, Q.C. (1997) The geochemistry and genesis of the Laoshan granitoids, Shandong Province. *Geological Journal of China Universities*, **3,** 1–15 [Chinese with English abstract].

Zhou, X.M. and Li, W.X. (2000) Origin of Late Mesozoic igneous rocks in Southeastern China: implications for lithosphere subduction and underplating of mafic magmas. *Tectonophysics*, **326**, 269–287.

Zhou, X.R. and Wu, K.L. (1994) *Zhangzhou Composite Granite*. Science Press, Beijing, China, pp. 1–53 [Chinese with English abstract].

[*Manuscript received 30 October 2005: revised 18 February 2007*]